

A&A manuscript no.
 (will be inserted by hand later)
Your thesaurus codes are:
06 (03.11.1; 16.06.1; 19.06.1; 19.37.1; 19.53.1; 19.63.1)

**ASTRONOMY
 AND
 ASTROPHYSICS**

ESO Imaging Survey

IV. Exploring the EIS Multicolor Data

S. Zaggia^{1,2}, I. Hook¹, R. Mendez^{1,3}, L. da Costa¹, L.F. Olsen^{1,4}, M. Nonino^{1,5}, A. Wicenec¹, C. Benoit^{1,6}, E. Deul^{1,7}, T. Erben^{1,8}, M.D. Guarneri^{1,9}, R. Hook¹⁰, I. Prandoni^{1,11}, M. Scodéggi¹, R. Slijkhuis^{1,7}, and R. Wichmann^{1,12}

¹ European Southern Observatory, Karl-Schwarzschild-Str. 2, D-85748 Garching b. München, Germany

² Osservatorio Astronomico di Capodimonte, via Moiariello 15, I-80131. Napoli, Italy

³ Cerro Tololo Inter-American Observatory, Casilla 603, La Serena, Chile

⁴ Astronomisk Observatorium, Julianne Maries Vej 30, DK-2100 Copenhagen, Denmark

⁵ Osservatorio Astronomico di Trieste, Via G.B. Tiepolo 11, I-31144 Trieste, Italy

⁶ DAEC, Observatoire de Paris-Meudon, 5 Pl. J. Janssen, 92195 Meudon Cedex, France

⁷ Leiden Observatory, P.O. Box 9513, 2300 RA Leiden, The Netherlands

⁸ Max-Planck Institut für Astrophysik, Postfach 1523 D-85748, Garching b. München, Germany

⁹ Osservatorio Astronomico di Pino Torinese, Strada Osservatorio 20, I-10025 Torino, Italy

¹⁰ Space Telescope – European Coordinating Facility, Karl-Schwarzschild-Str. 2, D-85748 Garching b. München, Germany

¹¹ Istituto di Radioastronomia del CNR, Via Gobetti 101, 40129 Bologna, Italy

¹² IUCAA, Post Bag 4, Ganeshkhind, Pune 411007, India

Received ; accepted

Abstract. This paper presents preliminary lists of potentially interesting point-like sources extracted from multicolor data obtained for a 1.7 square degree region near the South Galactic Pole. The region has been covered by the ESO Imaging Survey (EIS) in B , V and I and offers a unique combination of area and depth. These lists, containing a total of 330 objects nearly all brighter than $I \sim 21.5$, over 1.27 square degrees (after removing some bad regions), are by-products of the process of verification and quality control of the object catalogs being produced. Among the color selected targets are candidate very low mass stars/brown dwarfs (54), white-dwarfs (32), and quasars (244). In addition, a probable fast moving asteroid was identified. The objects presented here are natural candidates for follow-up spectroscopic observations and illustrate the usefulness of the EIS data for a broad range of science and for providing possible samples for the first year of the VLT.

Key words: imaging survey – color catalog – quasars

1. Introduction

The present paper is the fourth of a series presenting the data accumulated by the public ESO Imaging Survey (EIS), being carried out in preparation for the first year of regular operation of the VLT. As described in previous papers (Renzini & da Costa 1997, Nonino *et al.* 1998, hereafter paper I) the main goals of the EIS project are to conduct an imaging survey suitable for finding “rare” objects for follow-up observations with the VLT and to lay down the groundwork for more ambitious

wide-field digital, multicolor imaging surveys. The adopted strategy was designed to search for distant clusters of galaxies, quasars, high-redshift galaxies and to identify rare stellar types.

As part of EIS-wide, observations were obtained in three passbands (B , V and I) over an area of about 1.7 square degrees in a region near the South Galactic Pole (EIS-wide patch B). The region was selected because of the high density of known intermediate red-shift quasars. The multicolor data for patch B are now being released and in a separate paper the observations, calibration and the overall quality of the data are described (Prandoni *et al.* 1998, paper III). In that paper, preliminary single passband catalogs were presented and evaluated by comparing the star- and galaxy-counts with models and results from other surveys and the EIS patch A, presented in paper I. The good agreement found from these comparisons indicates that the available data, reduction procedures and object catalogs extracted in each of the passbands are reliable. Furthermore, comparison of the observed color distribution for point-like sources, derived from a preliminary version of a color catalog, with predictions of galactic models also shows reasonable agreement.

Although encouraging, the above results do not fully characterize the color catalog, in particular if it is to be used to identify different types of objects based on color selection criteria. Target selection based on the location of objects in color-color space, require a careful investigation of the performance of the pipeline since any problem may lead to objects with spurious colors. Colors are sensitive to a number of effects such as the observing conditions, the photometric and astrometric solutions in the different passbands and the de-blending algorithm.

In order to have a better understanding of the impact of these effects in the color catalog, in this paper the $(B - V)$ versus $(V - I)$ diagram for point-sources is used to select objects lying in potentially interesting regions of color-color space. These objects, examined individually, are used to generate preliminary lists of candidates for different type of objects. The criteria adopted are conservative and not optimal but the results serve to illustrate the type of objects one may expect to find and the approximate size of candidate samples for follow-up spectroscopic observations. Since the data are public, improved selection can be carried out by other interested groups.

The goals of the present paper are: 1) to test the performance of the EIS pipeline in the production of object catalogs; 2) to assess the reliability of the color catalogs being extracted from the EIS multicolor data; 3) to provide ESO users with lists of potential VLT targets.

In section 2, the basic characteristics of the color catalog relevant to the present work are described. In section 3, the color-color diagram for point-like sources is inspected and empirical color criteria are used to generate a preliminary list of candidate white-dwarfs, low mass stars and quasars, with a range of redshifts. Results and the outlook for the future is presented in section 4.

2. The Point-Source Color Catalog

The color catalog described here has been constructed from objects detected in the 150 sec exposures using multicolor data presented in paper III. Color catalogs extracted from the co-added images will only be available in the final release.

As discussed in paper III, the generation of a color catalog for generic use is a complex task given the range of possibilities in its definition, which depends to a large extent on the science goals. Since the intention of the present paper is primarily to understand some general characteristics of the color catalog and evaluate its usefulness for the primary science goals of the survey, the following prescription has been adopted. Starting from the unique catalogs covering the whole patch extracted from the best available images in each passband (see paper III), a color catalog is created by associating the objects detected in the different passbands (see paper I). The final product is a unique entry for each object, listing the photometric parameters and flags for each detection in each passband, and information about the best seeing frames in all bands. This information allows limits on the color for objects not detected in some of the passbands to be calculated. At this point all detections are considered, regardless of the band in which they were detected and the nature of the object (star/galaxy).

It has been found, for instance, that this catalog contains objects detected in the blue passbands without counterparts in V and I . Visual inspection of some of these cases, which represent roughly 2% of the total number of objects for $B \lesssim 22$, shows that the unusual colors observed come mostly from objects detected at the border of individual frames or along diffraction spikes of bright stars. Others are due to ghost images present in the B and V images (see paper III) and to merged images

that are de-blended in some passbands and not in others, depending on the seeing. Even though this is the most general color catalog, it is not the most convenient catalog to use. This is especially the case for extended objects for which are contaminated by the problems mentioned above and for which one would like to have the object centroid and measure magnitudes with the same aperture in all bands. Another problem is that the star/galaxy classification may vary from band to band, thus implying that the object classification may not be unique.

To avoid some of these ambiguities, this paper considers only point-sources as defined in the I -band. The selected sample includes only objects detected in the I -band brighter than $I = 23.0$ and with SExtractor stellarity index ≥ 0.75 . In addition, all objects with non-zero SExtractor and WeightWatcher flags (paper I) are removed from the catalog, in order to minimize contamination by spurious extreme color objects, which originate from some of the cases described above. It is worth pointing out that by eliminating all these objects a priori may discard some interesting cases. The final sample is available at "<http://www.eso.org/eis/>".

Note that star/galaxy classification is only reliable for magnitudes brighter than $I \sim 21.5$ and colors were computed using the mag_auto estimator introduced in paper I. The mean error in the colors are less than 0.15 mag for sources brighter than the star-galaxy separation limit, and about 0.4 mag near the limiting magnitude of the sample.

Since the primary goal of this paper is to illustrate the possible use of EIS data for different science goals and to evaluate the size of interesting samples for follow-up work, the criteria adopted have been in general conservative. In particular, in the selection of targets discussed below only reliable I -band detections, with $\epsilon_I \lesssim 0.2$ ($S/N \gtrsim 5$) are considered. Furthermore, to avoid regions of very poor seeing and low transparency, some regions were discarded, based on the distributions of seeing and limiting isophotes shown in paper III, leading to a sample covering a total area of 1.27 square degrees (e.g., figure 4).

To illustrate the general properties of the sample the color-magnitude diagrams V versus $(B - V)$ and V versus $(V - I)$ are shown in figure 1 for 3233 point-sources with $S/N \gtrsim 5$ in the I passband. The color distribution for sources brighter than $V = 21$ has already been discussed in paper III and compared with model predictions. This plot is presented in V -band to make the comparison with other works easier (e.g., Reid and Majewski 1993). Note that at faint magnitudes ($V \gtrsim 21$) incompleteness in the stellar sample sets in (see paper III). In the figure blue, $(B - V) \sim 0.5$, and red, $(B - V) \sim 1.5$ concentrations are clearly seen for $V \gtrsim 18.5$. This reflects the typical bimodal color distribution observed for faint stars at high-galactic latitude, with the blue peak arising from the turnoff of the main sequence for low-metallicity halo stars and the red peak from disk stars. Note that the blue peak is well-defined in the magnitude range $18.5 < V < 21.5$. For fainter magnitudes it fades away partly due to the incompleteness of the catalog and partly because at this magnitude limit one is approaching the outer parts of the halo.

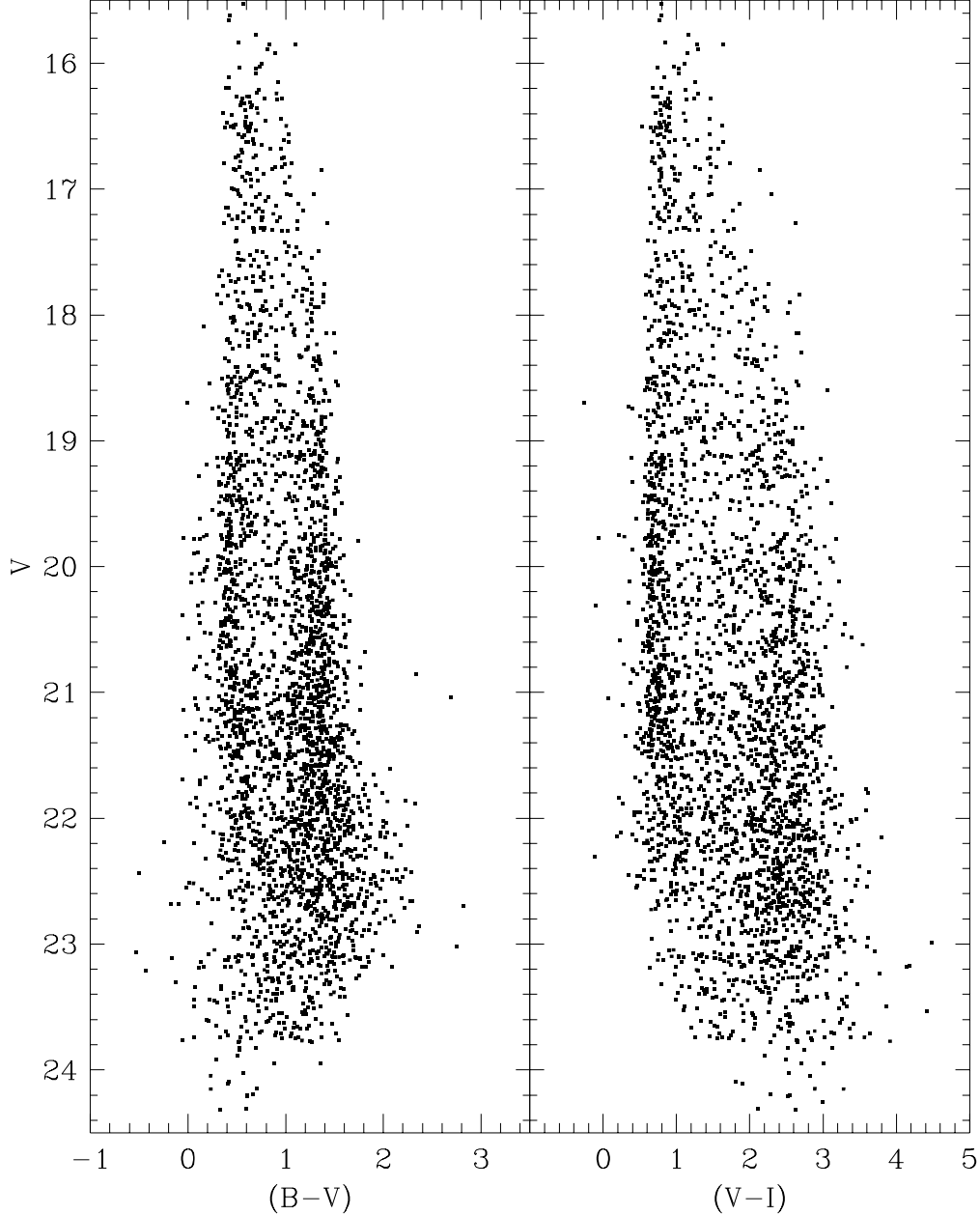


Fig. 1. Color-magnitude diagrams for EIS point-like sources.

From the figure one sees that for $V \gtrsim 19$ there is a large number of objects bluer than the concentration associated with the halo stars, and for $V \gtrsim 21.5$ there is a population of very red objects with $(V - I) > 3.5$. Both are examples of interesting populations, the identification of which is better explored using the color-color diagram as discussed in the following section.

3. Target Selection

Figure 2 shows the color-color diagrams for the 3233 objects detected ($S/N > 5$) in the I passband and the 345 objects detected in V and I only ($S/N > 5$). The plot includes all objects brighter than $I = 23$. For non-detections in B (hereafter B-dropouts) an estimate of the B limiting magnitude has been

measured on the best seeing frame. The limiting magnitude is defined to be a 1σ detection within the area corresponding to the seeing-disk as measured in the I -band. From this an estimate of the lower limit on the $(B - V)$ color is calculated. In addition to the B-dropouts, there are objects only detected in the I -band, for which the lower limit in $(V - I)$ is similarly computed. While a large number of these objects is expected if one considers the sample as a whole (because of the relative bright limiting magnitudes of the V images), objects brighter than $I \sim 21$ are the most interesting and are the ones considered in more detail below.

For comparison with the previous figures, figure 3 shows the locus of main sequence, giants, white dwarf and brown dwarf stars. The stellar locus for main sequence, subgiant- and

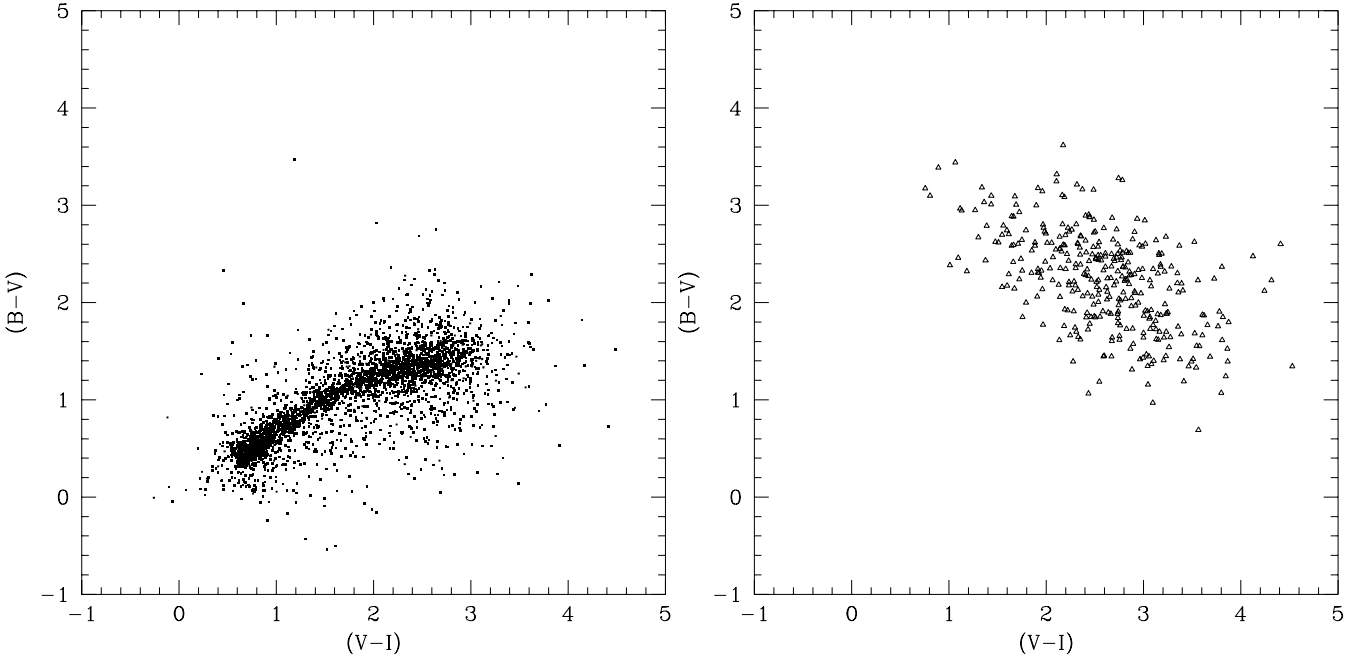


Fig. 2. Color-color diagram for EIS point-sources. Left-panel: those detected in all three passbands. Right-panel: those detected in V and I but not B , for which the lower limit in $(B-V)$ is indicated.

red-giant branch stars typical of the old low-metallicity halo and the young solar-type metallicity disk was taken from the models of Bertelli *et al.* (1994) extending down to $0.6 M_{\odot}$. The color-color cooling sequence for pure-Hydrogen WD was taken from Bergeron, Wesemael, & Beauchamp (1995). Finally, the locus for very low mass stars and/or brown dwarfs down to $0.08 M_{\odot}$ is taken from the models of Baraffe *et al.* (1998). These curves are presented in the Jonhson-Cousins system, close to the EIS magnitude system except for the B -band (paper III). However, the differences are relatively small and have no significant impact on the adopted selection criteria described below.

Also shown in figure 3 is the track of quasars in the color-color diagram as a function of redshift and the typical color scatter along the sequence due to the different assumptions for their typical spectra and intervening absorption. QSO colors were simulated using synthetic QSO spectra, which cover a range of intrinsic properties, and the response functions of the EIS filters (paper I). The method is the same as that used by Warren, Hewett & Osmer (1994) and Hall *et al.* (1996), and is a modified version of the method of Warren *et al.* (1991). QSO spectra were synthesised assuming that the QSO continuum has the form of a single power law with spectral index α ($S(v) \propto v^{\alpha}$) and assuming fixed emission line strengths relative to Ly α +NV. Three different values of the spectral index $\alpha = (-0.25, -0.75, -1.25)$ were used, and three different values for the emission line strength, defined by the Ly α +NV rest-frame equivalent width, $EW(\text{Ly}\alpha+\text{NV})=(42, 84 \text{ and } 168 \text{ \AA})$. For each set of assumptions, spectra were generated at intervals of 0.1 in z over the range $(3.0 < z < 5.0)$. Absorption by intervening HI was taken into account by simulating absorption spectra,

following the method of Warren, Hewett & Osmer (1994) and based on the work of Møller and Jacobsen (1990). For each set of intrinsic properties, ten QSO spectra were generated at each z step, each using a different realization of the absorption spectrum appropriate for that redshift. Thus at each redshift a total of 90 spectra were generated. Because patch B is close to the South Galactic Pole galactic extinction was neglected in the present calculation. Figure 3 shows the median and the scatter corresponding to the various simulations as a function of redshift.

In addition, in figure 3 all the 19 known quasars present in the field are shown in their measured EIS magnitudes. These quasars have redshifts, taken from the literature, in the range $0.4 < z < 2.96$.

Comparison of the color-color diagram for the data and model predictions shows at least four regions of potential interest. These regions are schematically shown in figure 3 and their limits are given in table 1. Objects in region I are candidate very low mass stars (VLM) or brown dwarf stars (BD), those in region II are candidate white dwarfs (WD). Candidate quasars (QSO) at different redshifts should lie in regions III and IV. Below preliminary lists for these objects are presented in tables which give: in column (1) the object name; in columns (2) and (3) the J2000 coordinates; in columns (4) and (5) the I magnitude and its error estimate ϵ_I ; in columns (6) and (7) the $(B-V)$ color and its error estimate $\epsilon_{(B-V)}$; in columns (8) and (9) the $(V-I)$ color and its error estimate $\epsilon_{(V-I)}$; and in column (10) notes or comments on the individual objects, whenever necessary. In the cases where the $(B-V)$ and/or $(V-I)$ colors are lower limits, the measure is preceded by a $>$ sign and the error in the color is the error in the magnitude in the passband

Table 1. Definition of regions of interest in figure 3 for candidate objects.

Region	Cand. Objects	Definition
I	VLM/BD	$(V - I) \geq 3.5$
II	WD	$(V - I) \leq 0.5$ and $(B - V) \leq 0.5$
III	QSO	$\begin{cases} -0.25 < (V - I) < 0.5 \text{ and } (B - V) > 0.5 \\ 0.5 < (V - I) < 2.0 \text{ and } (B - V) > 0.86(V - I) + 0.29 \\ 2.0 < (V - I) < 3.5 \text{ and } (B - V) > 2.0 \end{cases}$
IV	QSO Low z	$0.5 < (V - I) < 1.0$ and $-0.25 < (B - V) < 0.25$

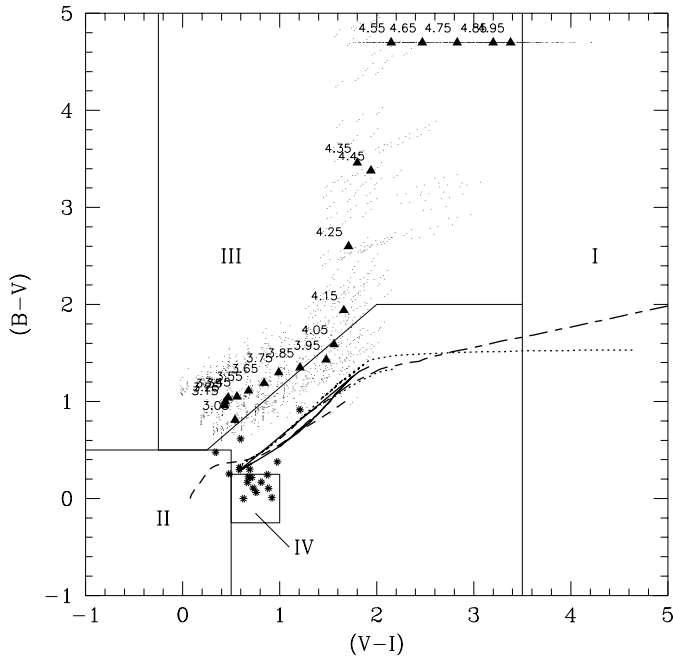


Fig. 3. Theoretical color-color plot for different type of objects. The solid line shows the location of main sequence, sub- and red-giant branch stars of an old halo, low metallicity, stellar population model taken from Bertelli *et al.* (1994). The dotted line shows the location of main sequence, sub- and red-giant branch stars of a young disk, solar metallicity, stellar population model taken from Bertelli *et al.* (1994). The short-dashed line shows the location of a WD pure Hydrogen cooling sequence taken from Bergeron, Wesemael, & Beauchamp (1995). The long-dashed line shows the location of 5 Gyr old BD stars with solar metallicity, taken from Baraffe *et al.* (1998). The color track for QSOs at different redshifts ($3.05 < z < 5.00$) are shown by triangles while the dots indicate the typical scatter around the median for the different parameters of the spectral properties and absorbers of high-redshift quasars (see text). Also shown (stars) are the EIS colors of the known quasars present in the EIS catalog which have redshifts in the range $0.4 < z < 2.96$.

in which the object is detected. For objects not detected in two passbands the error in the color is set to zero in the tables.

3.1. Rare Stellar-type Candidates

One of the interesting regions of the color-color diagram is the region redder than $(V - I) \geq 3.5$ (region I). Objects in this region extend well beyond the track defined by main-sequence stars with masses greater than $0.6M_{\odot}$. Therefore, this region should be populated primarily by very low mass stars ($0.6 > M/M_{\odot} > 0.1$) in the disk and/or brown dwarfs. Another possibility is that they are asymptotic giant and red giant branch stars. However, this is unlikely because there should be few of them in this color and magnitude range since they would have to be high metallicity objects at very large distances from the Sun (~ 100 kpc). Even though unlikely, considering the size of the area covered by the EIS multicolor data, this region of the color space could also be populated by very high-redshift QSOs with very large $(B - V)$, which could appear as B non-detections. In this region there are 18 detections (listed in table 2); 22 B-dropouts with $(V - I) \geq 3.5$, all brighter than $I = 20$ (listed in table 3); and 14 objects with $I \lesssim 21$, which are only detected in the I -band (listed in table 4). In the tables with “rare” stellar objects (2, 3, and 4), the following naming convention has been adopted: VLM, for very low mass candidates, VLMB, for very low mass B-dropouts, and VLMI, for the objects only detected in the I -band.

Since extreme colors could be caused by some unexpected artifact all these cases have been visually inspected, and all seem to be legitimate candidates. Note, however, that in the course of the inspection the two brightest objects in this sample exhibited a strange morphology in the coadded image appearing to be a “double” star, with the two objects having almost exactly the same magnitude, $I = 17.46 \pm 0.01$, and a few arcsecs of separation. This prompted the examination of the two single frames, which showed a single slightly elongated object that occupies different positions in the two single exposure images. The object was observed at $\alpha = 00^{\circ}49'37''$.71, $\delta = -29^{\circ}50'58''.7$, $JD = 50696.3174202$ and $\alpha = 00^{\circ}49'37''$.76, $\delta = -29^{\circ}50'56''.7$, $JD = 50696.32054438$. This fact strongly suggests that this object is probably a relatively fast moving asteroid. However, no known asteroids were found to be at the observed position during the nights the observations were conducted. This example of a serendipitous source demonstrates the need to implement tools in the EIS pipeline to search for transient phenomena present in the survey such as high proper-motion objects, variables, supernovae.

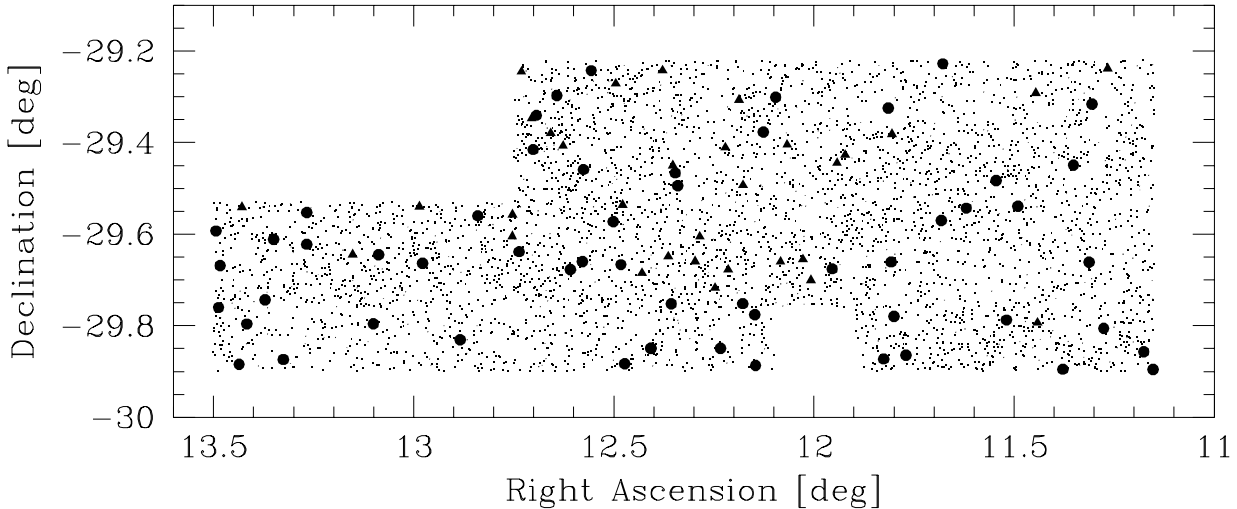


Fig. 4. Projected distribution of star-like objects which shows: all stellar objects detected in the selected area of patch B (dots); low-mass candidates found in region I of the color-color diagram of figure 3 (filled circles); and WD candidates in region II (filled triangles)

Another potentially interesting population is that defined by objects in region II of figure 3. These objects are clearly visible in figure 1 at magnitudes $V \gtrsim 19.5$. These blue objects could be either relatively hot (young) disk white dwarfs or blue horizontal branch (HB), low-metallicity halo stars. However, for $V \gtrsim 20$ HB stars would be located at $\gtrsim 100$ kpc, where the density should be extremely small for standard galactic structure models. There are 32 objects in region II which are listed in table 5. The adopted cut-off in $(V - I)$ (see table 1) was chosen based on cooling sequence of disk white dwarfs (Bergeron, Wesemael, & Beauchamp 1995) shown in figure 3. We emphasize that the criterion adopted is somewhat arbitrary and it is used simply to illustrate the possible identification of these objects. As can be seen from figure 3, this sample can be contaminated by low redshift quasars. In fact table 5 contains 2 already known quasar which are identified (name and redshift from the Simbad database). The U -band data will be useful to sort out these cases.

Finally, figure 4 shows the spatial distribution of these various candidates. Note that the northeast edge of the patch has been removed because of the incompleteness of the B-band catalogs. Similarly, a region along the southern edge was removed because of the incompleteness in the I-band catalog. A small trimming of the whole region has also been done yielding a total area of 1.27 square degrees.

3.2. Quasar Candidates

From simulations of QSO tracks (figure 3) high redshift QSOs ($3 < z < 5$) can be found in region III of the color-color diagram, while the available sample of known low redshift QSOs populate region IV (see figure 3, Osmer *et al.* 1998). The rough criteria used to define region III (table 1) were chosen based on the simulated QSO track. The blue part was chosen to be parallel to the stellar locus but shifted to minimize the contamination by stars. Several improvements in the selection can be made to take into account the errors in colors, as a function of the magnitude, and to optimize the yield based on the expected density of objects of different types. Since the parent sample is public, interested groups are likely to make significant refinements to the selection criteria adopted here.

In region III there are 70 objects detected in all three passbands. These are listed in table 6. In addition, there are 126 objects that are detected in V and I but not detected in B (hence have lower limits in $(B - V)$) that could also lie in region IV. These objects are listed in table 7. Note that, since the depth of the B images varies across the patch, the limits on $(B - V)$ are more meaningful in some areas than others. The depth of the B frames corresponding to each object can be calculated from the V magnitude and the $(B - V)$ limits given in table 6. In the tables the following naming convention has been adopted: QSO and QSOB stand for objects in region III detected in all three bands ($\gtrsim 3.0$) and B-dropouts candidates, respectively.

Adopting the criteria given in table 1 for region IV, where QSOs with $z \lesssim 3$ are likely to be found, one finds 48 stellar objects which are listed in table 8. This table includes 6 known QSOs, as indicated (name and redshift are from the Simbad database). In the table QLZ stands for low redshift ($z \lesssim 3.0$) quasars. Note, however, that with the follow-up observations in U -band to be carried out later this year, it will be possible to select low-z QSOs more efficiently.

Figure 5 show the projected sky distribution of the QSO candidates. This figure should be compared with those for the seeing and the limiting magnitudes presented in paper III to investigate possible correlations between the QSO candidates and the quality of the data, especially the B-dropouts or those detected only in the I-band. At first glance there is no obvi-

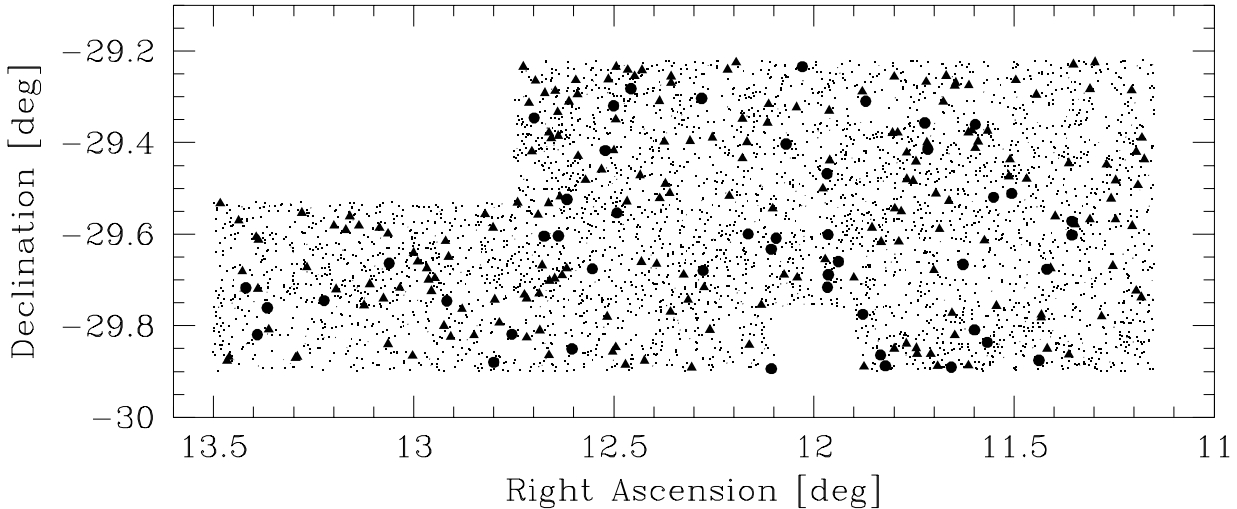


Fig. 5. Projected distribution of quasar candidates at low (filled circles), intermediate and high redshift (filled triangles). The adopted selection criteria are discussed in the text.

ous correlation as the QSO candidates seem to be uniformly distributed over the surveyed area.

4. Summary and Outlook

The ESO Imaging Survey is being carried out to help the selection of targets for the first year of operation of VLT. This paper presents some examples of possible candidates of interest, giving special emphasis to stellar populations and quasars. Using the area covered by the survey one is able to find candidate WDs and red objects likely to be associated with very low mass stars or brown dwarfs. A preliminary list is also presented for quasars. These lists and image postage stamps in all three passbands are also available in the ESO Science Archive server which allows the examination of the candidates ([“\[http://www.eso.org/eis/”\]\(http://www.eso.org/eis/\)](http://www.eso.org/eis/)). Finding charts can also be easily extracted. Also available is the parent color sample from which these candidates have been defined. It is important to emphasize that in addition to providing these preliminary lists, the present work has been an essential part in understanding the characteristics of the color catalogs being produced and for the verification of their reliability.

Improvements in the sample selection are certainly possible. Since the data are publicly available, interested groups may refine the selection criteria and produce their own samples. The present results lead to samples that are of the order of 50 to 100 candidates each. The yield will only be defined by follow-up spectroscopic observations. Much larger samples will be available from the Pilot Survey to be carried out with the new wide-field camera (mecWIDE) on the 2.2 m telescope at La Silla.

The present exploratory work has been done on a relatively small sample with preliminary selection criteria and by handling the data in a standard way. Nevertheless, it has already demonstrated the need for providing users with more information than possible with traditional catalogs, as emphasized by several other groups. The exercise points out the need for the

development of an object-oriented database and tools to inspect the multi-dimensional space of magnitudes, colors and extraction parameters. In addition, full exploration of the data also requires tools to facilitate the cross-identification of detected objects with available databases in other wavelengths and with spectral information, and to handle time-dependent information obtained in the course of deep surveys.

The integration of EIS and the program being developed by the ESO Science Archive Group is an essential step in the process of translating results from multicolor deep (co-added) imaging surveys into target lists for the VLT. The Pilot Survey to be conducted on the 2.2m telescope early next year offers the ideal test case to define the basic science-driven requirements for data mining the associated database. However, in order to take full advantage of the new opportunities in a timely fashion, as required to support VLT-science, a significant effort must be made well beyond what has been done for EIS. As generally recognized, the coming of age of large, digital, multicolor imaging surveys creates new demands for more efficient ways of extracting information. The development of these tools and of efficient unsupervised pipelines is currently the major challenge for the optimal extraction of valuable scientific results.

Acknowledgements. We thank all the people directly or indirectly involved in the ESO Imaging Survey effort. In particular, all the members of the EIS Working Group for the innumerable suggestions and constructive criticisms, the ESO Archive Group and the ST-ECF for their support. Special thanks to A. Baker and D. Clements for their contribution in the quasar search in the early stages of the EIS project. We would also like to thank S. Warren for helpful comments and providing the code for the calculation of the color track for quasars for the EIS filters and I. Baraffe for providing the locus of brown dwarfs in the appropriate passbands. Our special thanks to the efforts of A. Renzini, VLT Programme Scientist, for his scientific input, support and dedication in making this project a success. Finally, we would like to thank ESO’s Director General Riccardo Giacconi for making this effort possible in the short time available. This research has made use of the

Simbad database, operated by the Centre de Donnes astronomiques de Strasbourg.

References

- Baraffe I., Chabrier G., Allard F., & Hauschildt P. H., 1997, A&A in publication
- Bertelli G., Bressan A., Chiosi C., Fagotto F., & Nasi E., 1994, A&ASS, 106, 275
- Bergeron P., Wesemael F., & Beauchamp A., 1995, PASP, 107, 1047
- Boyle B.J. 1989, MNRAS, 240, 533
- Hall P.B., Osmer P.S., Green R.F., Porter A.C., & Warren S.J. 1996, ApJ, 462, 614
- Møller P., Jakobsen P., 1990, A&A, 228, 299
- Nonino M., Bertin E., da Costa L., Deul E., Erben T., Olsen L., Prandoni I., Scodéggi M., Wicenec A., Wichmann R., Benoist C., Freudling W., Guarneri M. D., Hook I., Hook R., Mendez R., Savaglio S., Silva S., Slijkhuis S., 1998, A&A submitted, astro-ph/9803336, paper I
- Osmer P.S., Kennefick J.D., Hall P.B., & Green R.F., 1998, ApJ in publication, astro-ph/9806366
- Prandoni I., *et al.*, 1998, A&A submitted, paper III
- Renzini A., & da Costa L., 1997, The Messenger, 87, 23
- Reid N., & Majewski, S.R. 1993, ApJ, 409, 635
- Warren S. J., Hewett P. C., Osmer P. S., 1994, ApJ, 421, 412
- Warren S. J., Hewett P. C., Irwin M. J., Osmer P. S., 1991, ApJS, 76, 1

Table 2. Very Low-Mass Star Candidates.

ID	α (J2000.0)	δ	I	ϵ_I	(B-V)	$\epsilon_{(B-V)}$	(V-I)	$\epsilon_{(V-I)}$
EIS VLM 1	004530.77	-295341.8	19.04	0.01	1.82	0.41	4.14	0.19
EIS VLM 2	004557.66	-293220.1	19.36	0.02	0.89	0.41	3.70	0.26
EIS VLM 3	004713.69	-293938.1	19.00	0.02	1.36	0.46	4.17	0.22
EIS VLM 4	004715.38	-291927.6	18.17	0.01	1.79	0.29	3.59	0.08
EIS VLM 5	004749.07	-294032.3	19.46	0.02	0.96	0.37	3.77	0.16
EIS VLM 6	004923.17	-292758.6	19.11	0.02	0.72	0.44	4.42	0.19
EIS VLM 7	004953.47	-295258.9	17.08	0.00	1.55	0.10	3.54	0.02
EIS VLM 8	005000.31	-293421.9	19.33	0.01	1.55	0.42	3.62	0.15
EIS VLM 9	005018.26	-292731.2	18.34	0.01	1.59	0.25	3.59	0.06
EIS VLM 10	005026.08	-294038.3	20.07	0.03	1.52	0.46	3.64	0.25
EIS VLM 11	005056.76	-293817.5	18.18	0.01	1.99	0.21	3.62	0.07
EIS VLM 12	005304.15	-293719.4	18.50	0.01	1.52	0.29	4.49	0.13
EIS VLM 13	005318.17	-295225.2	18.81	0.01	2.28	0.39	3.62	0.10
EIS VLM 14	005324.08	-293640.7	19.86	0.02	0.53	0.34	3.91	0.22
EIS VLM 15	005344.66	-295303.5	18.94	0.01	1.58	0.25	3.60	0.12
EIS VLM 16	005356.07	-294007.4	19.42	0.02	1.14	0.35	3.60	0.26
EIS VLM 17	005357.00	-294536.7	20.18	0.04	1.13	0.48	3.56	0.27
EIS VLM 18	005358.58	-293534.5	19.62	0.02	1.35	0.49	3.87	0.29

Table 3. Very Low-Mass Star Candidates B-dropout.

ID	α (J2000.0)	δ	I	ϵ_I	(B-V)	$\epsilon_{(B-V)}$	(V-I)	$\epsilon_{(V-I)}$
EIS VLMB 1	004442.23	-295124.4	20.62	0.05	> 1.87	0.43	3.61	0.44
EIS VLMB 2	004506.24	-294820.5	20.73	0.05	> 1.76	0.29	3.77	0.29
EIS VLMB 3	004513.27	-291857.3	20.92	0.12	> 1.07	0.47	3.80	0.48
EIS VLMB 4	004604.51	-294715.3	20.19	0.03	> 2.25	0.28	3.73	0.28
EIS VLMB 5	004610.71	-292858.7	19.84	0.02	> 2.23	0.17	3.56	0.17
EIS VLMB 6	004628.66	-293236.0	20.16	0.03	> 1.77	0.36	3.66	0.36
EIS VLMB 7	004643.65	-293413.2	19.87	0.03	> 1.34	0.37	4.53	0.37
EIS VLMB 8	004704.82	-295151.0	19.43	0.02	> 2.23	0.23	4.32	0.23
EIS VLMB 9	004830.31	-292237.1	18.98	0.01	> 2.37	0.11	3.81	0.11
EIS VLMB 10	004834.99	-295313.0	20.47	0.05	> 1.42	0.33	3.51	0.34
EIS VLMB 11	004835.42	-294632.0	19.76	0.04	> 1.85	0.25	3.82	0.26
EIS VLMB 12	004842.70	-294506.5	20.76	0.08	> 1.44	0.38	3.69	0.39
EIS VLMB 13	004921.62	-292937.8	20.68	0.05	> 1.55	0.27	3.58	0.27
EIS VLMB 14	004925.57	-294508.3	20.88	0.06	> 1.66	0.32	3.61	0.33
EIS VLMB 15	005018.77	-293934.8	19.02	0.01	> 2.60	0.19	4.41	0.19
EIS VLMB 16	005034.15	-291749.1	18.49	0.01	> 2.48	0.12	4.12	0.12
EIS VLMB 17	005046.36	-292025.1	19.79	0.03	> 1.24	0.21	3.85	0.21
EIS VLMB 18	005048.39	-292454.2	19.40	0.02	> 2.62	0.14	3.52	0.14
EIS VLMB 19	005121.59	-293335.3	20.46	0.04	> 1.87	0.25	3.62	0.25
EIS VLMB 20	005154.63	-293948.9	20.40	0.04	> 1.80	0.24	3.88	0.25
EIS VLMB 21	005304.07	-293308.7	21.03	0.07	> 1.33	0.43	3.54	0.43
EIS VLMB 22	005340.06	-294746.9	20.30	0.04	> 1.91	0.24	3.78	0.24

Table 4. Very Low-Mass Star Candidates, only detected in the I -band.

ID	α (J2000.0)	δ	I	ε_I	(B-V)	$\varepsilon_{(B-V)}$	(V-I)	$\varepsilon_{(V-I)}$
EIS VLMI 1	004436.65	-29 53 44.9	20.91	0.06	> 0.56	0.00	> 4.73	0.06
EIS VLMI 2	004515.04	-29 39 40.8	20.77	0.08	> 0.39	0.00	> 4.84	0.08
EIS VLMI 3	004524.37	-29 26 57.3	20.76	0.05	> 0.32	0.00	> 4.80	0.05
EIS VLMI 4	004642.81	-29 13 40.4	20.87	0.08	> 0.43	0.00	> 4.61	0.08
EIS VLMI 5	004712.02	-29 46 46.0	20.55	0.05	> 0.39	0.00	> 5.14	0.05
EIS VLMI 6	004718.22	-29 52 21.0	20.81	0.06	> 0.44	0.00	> 4.89	0.06
EIS VLMI 7	004822.93	-29 18 03.9	20.72	0.06	> 0.06	0.00	> 4.87	0.06
EIS VLMI 8	004856.05	-29 50 56.8	20.58	0.14	> -0.26	0.00	> 4.89	0.14
EIS VLMI 9	004955.83	-29 39 59.6	20.89	0.06	> 0.37	0.00	> 4.89	0.06
EIS VLMI 10	005013.53	-29 14 34.1	20.25	0.04	> -0.23	0.00	> 5.24	0.04
EIS VLMI 11	005132.16	-29 49 51.6	20.98	0.06	> 0.54	0.00	> 4.64	0.06
EIS VLMI 12	005221.08	-29 38 41.0	20.90	0.06	> 0.37	0.00	> 4.83	0.06
EIS VLMI 13	005224.19	-29 47 43.8	20.86	0.06	> 0.53	0.00	> 4.83	0.06
EIS VLMI 14	005329.09	-29 44 35.2	20.02	0.03	> 0.55	0.00	> 5.42	0.03

Table 5. Candidate White Dwarfs

ID	α (J2000.0)	δ	I	ε_I	(B-V)	$\varepsilon_{(B-V)}$	(V-I)	$\varepsilon_{(V-I)}$	Notes
EIS WD 1	004503.90	-29 14 16.9	18.39	0.02	0.32	0.01	0.34	0.02	
EIS WD 2	004545.94	-29 47 36.4	18.93	0.01	0.32	0.01	0.40	0.01	
EIS WD 3	004546.93	-29 17 30.3	20.55	0.07	0.47	0.05	0.37	0.07	
EIS WD 4	004713.29	-29 22 52.4	21.04	0.07	0.20	0.06	0.30	0.08	
EIS WD 5	004741.21	-29 25 36.8	21.55	0.09	0.17	0.10	0.43	0.10	
EIS WD 6	004746.22	-29 26 39.5	20.96	0.07	0.39	0.08	0.48	0.08	
EIS WD 7	004801.88	-29 42 02.3	19.47	0.02	0.16	0.02	0.29	0.02	
EIS WD 8	004806.62	-29 39 18.0	19.84	0.03	-0.04	0.01	-0.07	0.03	
EIS WD 9	004815.99	-29 24 16.8	19.46	0.02	0.38	0.02	0.40	0.02	
EIS WD 10	004820.09	-29 39 36.7	20.83	0.06	0.08	0.04	0.27	0.07	
EIS WD 11	004842.47	-29 29 34.6	18.34	0.01	0.25	0.01	0.40	0.01	
EIS WD 12	004844.90	-29 18 24.0	19.96	0.03	0.47	0.04	0.47	0.04	
EIS WD 13	004851.47	-29 40 38.6	21.62	0.13	0.08	0.08	0.22	0.14	
EIS WD 14	004853.04	-29 24 37.5	20.61	0.05	0.40	0.05	0.48	0.06	
EIS WD 15	004859.20	-29 43 02.3	17.89	0.00	0.18	0.01	0.30	0.01	
EIS WD 16	004908.36	-29 36 18.4	19.75	0.02	0.45	0.02	0.37	0.03	
EIS WD 17	004911.34	-29 39 33.1	19.17	0.01	0.12	0.01	0.45	0.02	
EIS WD 18	004924.64	-29 26 59.4	19.94	0.04	0.28	0.03	0.34	0.04	
EIS WD 19	004927.36	-29 38 56.4	21.88	0.13	0.26	0.11	0.24	0.15	
EIS WD 20	004930.88	-29 14 33.6	20.99	0.07	0.33	0.09	0.44	0.08	
EIS WD 21	004943.17	-29 41 05.3	20.49	0.05	0.19	0.04	0.29	0.05	
EIS WD 22	004954.72	-29 32 10.0	20.87	0.05	0.07	0.05	0.46	0.06	
EIS WD 23	004958.70	-29 16 15.4	19.53	0.02	0.19	0.02	0.22	0.02	
EIS WD 24	005030.48	-29 24 24.8	20.41	0.04	0.10	0.03	-0.11	0.04	
EIS WD 25	005037.90	-29 22 45.6	18.96	0.01	-0.01	0.01	-0.26	0.01	ICS96 004812.3-293904
EIS WD 26	005049.29	-29 20 47.1	20.65	0.06	0.29	0.10	0.50	0.07	
EIS WD 27	005055.45	-29 14 40.6	21.62	0.12	0.02	0.22	0.27	0.14	
EIS WD 28	005100.78	-29 33 26.1	18.75	0.01	0.30	0.01	0.38	0.01	[CS83] 0048-2982, $z = 2.439$
EIS WD 29	005100.94	-29 36 15.6	20.00	0.02	0.38	0.03	0.46	0.03	
EIS WD 30	005156.64	-29 32 23.5	20.97	0.06	0.07	0.04	0.08	0.06	
EIS WD 31	005236.64	-29 38 40.6	21.24	0.08	0.18	0.08	0.44	0.09	
EIS WD 32	005342.87	-29 32 27.0	20.42	0.04	0.41	0.04	0.41	0.04	

Table 6. Quasar Candidates.

ID	α (J2000.0)	δ	I	ϵ_I	(B-V)	$\epsilon_{(B-V)}$	(V-I)	$\epsilon_{(V-I)}$
EIS QSO 1	004441.79	-29 26 10.9	21.78	0.13	1.36	0.29	0.71	0.16
EIS QSO 2	004443.33	-29 23 22.3	21.45	0.08	1.48	0.37	1.14	0.15
EIS QSO 3	004445.68	-29 29 35.1	21.60	0.10	1.00	0.21	0.60	0.13
EIS QSO 4	004446.71	-29 43 25.5	21.93	0.17	1.59	0.27	0.56	0.24
EIS QSO 5	004449.24	-29 34 55.8	20.15	0.04	2.14	0.29	2.26	0.11
EIS QSO 6	004459.01	-29 28 56.7	18.73	0.01	2.17	0.52	3.49	0.08
EIS QSO 7	004500.80	-29 40 09.1	20.68	0.07	2.02	0.30	2.11	0.15
EIS QSO 8	004501.81	-29 31 20.5	20.71	0.06	1.92	0.30	1.80	0.20
EIS QSO 9	004507.46	-29 46 45.8	21.85	0.12	1.42	0.38	1.23	0.25
EIS QSO 10	004514.51	-29 34 05.4	20.14	0.04	2.08	0.29	2.35	0.18
EIS QSO 11	004523.16	-29 34 45.3	20.70	0.06	1.34	0.15	0.98	0.11
EIS QSO 12	004524.25	-29 13 45.4	21.92	0.14	1.24	0.30	0.74	0.24
EIS QSO 13	004527.27	-29 26 42.6	21.79	0.11	1.66	0.39	0.91	0.18
EIS QSO 14	004540.05	-29 51 01.0	20.58	0.06	1.47	0.13	0.53	0.11
EIS QSO 15	004543.67	-29 46 53.1	21.67	0.11	1.09	0.19	0.67	0.18
EIS QSO 16	004543.68	-29 46 34.4	20.67	0.05	2.82	0.34	2.03	0.15
EIS QSO 17	004617.85	-29 36 50.2	21.35	0.09	1.83	0.37	1.76	0.23
EIS QSO 18	004627.15	-29 16 30.6	19.46	0.03	2.03	0.33	2.58	0.10
EIS QSO 19	004642.42	-29 18 39.0	19.02	0.03	2.07	0.29	2.58	0.08
EIS QSO 20	004644.64	-29 35 20.1	19.31	0.02	2.04	0.23	2.56	0.12
EIS QSO 21	004645.69	-29 53 17.7	20.38	0.05	2.75	1.04	2.64	0.27
EIS QSO 22	004646.81	-29 30 40.5	20.24	0.04	2.18	0.43	2.39	0.15
EIS QSO 23	004649.87	-29 51 44.0	22.10	0.18	0.84	0.22	0.35	0.26
EIS QSO 24	004658.17	-29 51 41.1	21.83	0.12	1.99	0.45	0.67	0.23
EIS QSO 25	004700.65	-29 29 01.3	20.81	0.06	1.02	0.15	0.62	0.10
EIS QSO 26	004704.48	-29 50 19.8	21.67	0.11	1.37	0.38	0.99	0.29
EIS QSO 27	004709.86	-29 22 40.5	21.73	0.10	1.42	0.26	0.40	0.13
EIS QSO 28	004711.39	-29 32 38.8	20.86	0.06	1.05	0.10	0.62	0.08
EIS QSO 29	004753.17	-29 39 18.8	18.89	0.01	2.04	0.22	3.22	0.08
EIS QSO 30	004754.67	-29 30 01.2	21.91	0.11	1.13	0.34	0.91	0.17
EIS QSO 31	004824.72	-29 32 38.1	20.41	0.04	0.82	0.04	0.40	0.04
EIS QSO 32	004851.66	-29 14 26.5	19.81	0.03	2.08	0.31	2.50	0.10
EIS QSO 33	004905.87	-29 42 59.1	19.74	0.02	2.20	0.26	2.73	0.11
EIS QSO 34	004915.26	-29 44 37.8	21.84	0.13	1.59	0.38	1.52	0.25
EIS QSO 35	004917.97	-29 41 18.0	20.57	0.05	1.50	0.17	1.39	0.09
EIS QSO 36	004926.05	-29 46 09.4	20.10	0.04	2.03	0.50	2.20	0.13
EIS QSO 37	004932.48	-29 31 18.1	19.41	0.02	2.21	0.38	3.29	0.14
EIS QSO 38	004952.12	-29 31 42.8	21.56	0.10	1.28	0.26	1.01	0.16
EIS QSO 39	004958.93	-29 50 48.0	18.57	0.01	2.68	0.29	2.47	0.04
EIS QSO 40	005004.00	-29 46 48.0	19.96	0.03	2.11	0.50	2.86	0.15
EIS QSO 41	005017.07	-29 28 53.4	19.40	0.02	2.03	0.37	2.88	0.09
EIS QSO 42	005026.94	-29 18 36.4	21.95	0.17	0.50	0.27	0.19	0.19
EIS QSO 43	005028.30	-29 40 29.9	20.66	0.05	1.88	0.36	1.82	0.12
EIS QSO 44	005032.21	-29 31 04.0	21.96	0.11	0.96	0.21	0.50	0.19
EIS QSO 45	005035.42	-29 41 47.7	21.10	0.07	1.62	0.26	1.34	0.17
EIS QSO 46	005038.87	-29 22 42.3	21.94	0.13	1.21	0.31	0.75	0.17
EIS QSO 47	005039.04	-29 31 56.3	21.45	0.10	1.31	0.33	1.10	0.18
EIS QSO 48	005042.90	-29 40 04.8	20.84	0.06	2.08	0.41	2.34	0.19
EIS QSO 49	005044.44	-29 48 37.4	20.33	0.04	2.28	0.44	2.33	0.17
EIS QSO 50	005112.46	-29 35 08.7	21.58	0.10	1.72	0.29	1.22	0.15
EIS QSO 51	005137.90	-29 49 26.9	21.73	0.11	0.75	0.26	0.45	0.27
EIS QSO 52	005139.14	-29 38 57.7	19.39	0.02	2.16	0.37	3.11	0.11
EIS QSO 53	005141.77	-29 48 00.4	20.35	0.04	1.27	0.05	0.23	0.05
EIS QSO 54	005147.19	-29 41 45.3	20.32	0.04	2.05	0.30	2.11	0.14
EIS QSO 55	005149.34	-29 43 26.1	20.03	0.03	2.29	0.40	2.63	0.13
EIS QSO 56	005151.09	-29 41 58.0	21.58	0.10	1.72	0.41	1.54	0.19
EIS QSO 57	005157.52	-29 39 35.2	20.27	0.04	2.35	0.55	2.63	0.19

Table 6. Continued.

ID	α (J2000.0)	δ	I	ε_I	(B-V)	$\varepsilon_{(B-V)}$	(V-I)	$\varepsilon_{(V-I)}$
EIS QSO 58	005200.10	-29 38 26.4	19.74	0.02	2.22	0.39	2.66	0.12
EIS QSO 59	005200.58	-29 51 55.4	19.94	0.03	2.13	0.38	2.54	0.23
EIS QSO 60	005215.43	-29 50 24.9	19.53	0.10	2.12	0.28	2.61	0.20
EIS QSO 61	005218.14	-29 44 25.2	19.42	0.02	0.84	0.03	0.57	0.02
EIS QSO 62	005220.53	-29 35 11.1	21.44	0.09	1.17	0.13	0.51	0.11
EIS QSO 63	005304.09	-29 40 21.9	19.64	0.02	2.24	0.35	2.42	0.08
EIS QSO 64	005307.12	-29 33 13.0	19.75	0.02	2.12	0.38	2.73	0.10
EIS QSO 65	005309.86	-29 52 04.1	19.26	0.02	2.02	0.27	3.40	0.12
EIS QSO 66	005342.79	-29 40 53.4	19.54	0.03	2.23	0.23	2.32	0.09
EIS QSO 67	005344.89	-29 34 13.2	20.68	0.05	2.36	0.50	2.18	0.20
EIS QSO 68	005350.63	-29 52 06.5	21.80	0.14	1.56	0.43	1.48	0.29
EIS QSO 69	005351.90	-29 52 35.8	19.47	0.02	2.00	0.26	2.55	0.11
EIS QSO 70	005355.95	-29 31 57.9	22.00	0.13	1.05	0.23	0.46	0.20

Table 7. Quasar Candidates (B-dropouts).

ID	α (J2000.0)	δ	I	ϵ_I	(B-V)	$\epsilon_{(B-V)}$	(V-I)	$\epsilon_{(V-I)}$
EIS QSOB 1	004443.60	-294415.6	20.94	0.08	> 2.29	0.41	2.88	0.41
EIS QSOB 2	004446.83	-292512.3	20.84	0.05	> 2.43	0.22	2.70	0.22
EIS QSOB 3	004449.53	-291709.5	20.43	0.13	> 1.89	0.29	3.24	0.31
EIS QSOB 4	004459.22	-293404.5	20.10	0.04	> 2.51	0.18	3.16	0.18
EIS QSOB 5	004504.54	-292652.9	20.64	0.07	> 3.00	0.20	1.90	0.21
EIS QSOB 6	004511.56	-291327.9	19.87	0.03	> 3.26	0.18	2.79	0.18
EIS QSOB 7	004514.48	-291658.2	20.92	0.11	> 2.57	0.30	2.35	0.32
EIS QSOB 8	004527.11	-295148.2	20.81	0.05	> 2.11	0.26	3.36	0.26
EIS QSOB 9	004535.39	-293339.5	20.62	0.05	> 2.88	0.22	2.45	0.23
EIS QSOB 10	004537.95	-294027.1	20.94	0.12	> 2.46	0.30	2.51	0.33
EIS QSOB 11	004546.59	-291744.2	20.87	0.13	> 1.96	0.27	2.88	0.30
EIS QSOB 12	004552.35	-292844.7	20.33	0.03	> 2.58	0.17	2.99	0.17
EIS QSOB 13	004559.03	-291550.4	20.53	0.10	> 2.73	0.19	2.50	0.22
EIS QSOB 14	004602.32	-292613.9	20.58	0.04	> 1.89	0.36	3.24	0.36
EIS QSOB 15	004603.03	-292824.6	20.35	0.04	> 2.51	0.16	2.85	0.16
EIS QSOB 16	004610.49	-294524.2	20.82	0.08	> 1.98	0.30	3.22	0.31
EIS QSOB 17	004615.88	-292226.7	20.89	0.05	> 2.39	0.15	2.35	0.16
EIS QSOB 18	004621.42	-292351.2	20.90	0.05	> 1.69	0.23	3.00	0.24
EIS QSOB 19	004623.17	-292442.5	20.04	0.04	> 2.29	0.14	2.91	0.14
EIS QSOB 20	004625.30	-292223.0	20.77	0.05	> 2.68	0.12	2.14	0.13
EIS QSOB 21	004627.31	-292240.1	20.48	0.04	> 2.45	0.14	2.69	0.14
EIS QSOB 22	004627.38	-295312.9	20.41	0.04	> 2.64	0.31	3.13	0.31
EIS QSOB 23	004635.01	-291610.1	20.55	0.08	> 2.90	0.17	2.44	0.18
EIS QSOB 24	004635.45	-291632.5	20.15	0.07	> 2.87	0.18	2.68	0.19
EIS QSOB 25	004635.55	-294914.4	20.77	0.06	> 2.72	0.24	2.49	0.25
EIS QSOB 26	004637.12	-294620.3	20.81	0.06	> 3.25	0.18	2.11	0.19
EIS QSOB 27	004639.14	-293137.9	20.80	0.06	> 2.59	0.24	2.19	0.25
EIS QSOB 28	004640.80	-291514.7	20.24	0.08	> 2.75	0.25	2.73	0.26
EIS QSOB 29	004648.08	-294043.9	20.46	0.07	> 2.65	0.20	2.89	0.21
EIS QSOB 30	004652.18	-292357.5	20.94	0.06	> 2.55	0.20	2.10	0.21
EIS QSOB 31	004652.77	-291602.0	20.71	0.09	> 2.32	0.24	2.86	0.25
EIS QSOB 32	004658.63	-295055.5	20.80	0.08	> 2.10	0.33	2.97	0.34
EIS QSOB 33	004658.86	-292628.7	20.05	0.03	> 2.50	0.16	3.19	0.16
EIS QSOB 34	004704.25	-292848.2	20.89	0.05	> 2.24	0.27	2.81	0.28
EIS QSOB 35	004704.44	-292518.8	20.76	0.05	> 3.14	0.16	1.96	0.16
EIS QSOB 36	004707.58	-293300.3	20.62	0.05	> 1.87	0.20	3.18	0.21
EIS QSOB 37	004709.19	-293658.3	20.42	0.04	> 3.32	0.19	2.11	0.19
EIS QSOB 38	004711.70	-295059.8	20.46	0.04	> 2.49	0.31	3.16	0.32
EIS QSOB 39	004711.71	-291521.8	20.21	0.09	> 2.39	0.27	3.17	0.28
EIS QSOB 40	004712.91	-292243.9	20.91	0.06	> 2.52	0.17	2.41	0.18
EIS QSOB 41	004719.76	-293701.4	20.72	0.06	> 2.27	0.26	2.78	0.26
EIS QSOB 42	004725.12	-293508.5	20.79	0.06	> 1.88	0.42	3.15	0.43
EIS QSOB 43	004729.97	-295322.3	20.43	0.05	> 3.16	0.23	2.37	0.23
EIS QSOB 44	004730.99	-291719.9	20.31	0.08	> 2.77	0.16	2.59	0.18
EIS QSOB 45	004735.96	-294142.4	20.86	0.06	> 2.50	0.19	2.73	0.20
EIS QSOB 46	004750.55	-292619.1	20.70	0.07	> 2.11	0.19	2.91	0.20
EIS QSOB 47	004750.86	-291949.7	20.45	0.04	> 3.11	0.11	2.16	0.11
EIS QSOB 48	004810.07	-294141.5	20.21	0.04	> 3.62	0.16	2.17	0.17
EIS QSOB 49	004810.48	-291921.9	20.57	0.06	> 2.73	0.12	2.24	0.14
EIS QSOB 50	004817.74	-294120.1	20.77	0.06	> 2.51	0.21	2.79	0.22
EIS QSOB 51	004827.26	-291857.3	20.81	0.06	> 1.70	0.24	3.24	0.25
EIS QSOB 52	004827.83	-292123.8	20.57	0.05	> 2.51	0.16	2.61	0.17
EIS QSOB 53	004831.62	-294515.9	20.52	0.05	> 1.67	0.32	3.39	0.32
EIS QSOB 54	004838.67	-295030.5	20.30	0.05	> 2.10	0.25	2.91	0.25
EIS QSOB 55	004840.04	-292356.0	19.93	0.04	> 2.50	0.10	2.67	0.10
EIS QSOB 56	004842.85	-292604.8	20.03	0.04	> 2.60	0.12	2.74	0.12
EIS QSOB 57	004842.93	-292052.4	20.60	0.05	> 2.57	0.22	2.49	0.23

Table 7. Continued.

ID	α (J2000.0)	δ	I	ϵ_I	(B-V)	$\epsilon_{(B-V)}$	(V-I)	$\epsilon_{(V-I)}$
EIS QSOB 58	004846.70	-29 13 31.0	19.62	0.02	> 2.58	0.14	3.37	0.14
EIS QSOB 59	004850.70	-29 31 00.7	20.96	0.06	> 2.60	0.20	2.33	0.21
EIS QSOB 60	004900.87	-29 23 20.1	20.98	0.08	> 2.71	0.14	2.00	0.16
EIS QSOB 61	004902.39	-29 48 32.0	20.91	0.11	> 3.18	0.15	1.92	0.19
EIS QSOB 62	004913.25	-29 53 29.1	20.53	0.06	> 2.24	0.27	2.83	0.28
EIS QSOB 63	004914.19	-29 23 47.1	19.64	0.03	> 2.46	0.08	2.73	0.09
EIS QSOB 64	004925.56	-29 16 11.0	20.98	0.06	> 2.61	0.19	2.06	0.20
EIS QSOB 65	004925.61	-29 15 20.9	20.19	0.04	> 2.23	0.17	3.07	0.17
EIS QSOB 66	004926.46	-29 30 36.8	20.81	0.05	> 2.37	0.26	2.67	0.26
EIS QSOB 67	004928.96	-29 29 23.8	20.27	0.03	> 2.37	0.18	3.18	0.18
EIS QSOB 68	004929.81	-29 23 53.5	20.55	0.06	> 1.37	0.20	3.09	0.21
EIS QSOB 69	004932.65	-29 18 32.3	20.25	0.04	> 2.41	0.14	2.84	0.15
EIS QSOB 70	004934.33	-29 39 53.7	20.46	0.04	> 2.59	0.19	2.96	0.20
EIS QSOB 71	004941.58	-29 52 35.2	20.42	0.04	> 2.88	0.14	2.44	0.15
EIS QSOB 72	004943.18	-29 14 30.5	20.68	0.05	> 1.39	0.42	3.50	0.43
EIS QSOB 73	004943.49	-29 39 38.5	20.58	0.05	> 2.14	0.26	3.27	0.27
EIS QSOB 74	004944.25	-29 28 16.9	20.07	0.04	> 1.92	0.19	3.08	0.19
EIS QSOB 75	004947.52	-29 15 17.0	20.36	0.04	> 2.81	0.12	2.31	0.13
EIS QSOB 76	004950.13	-29 16 56.0	20.54	0.05	> 2.33	0.17	2.59	0.17
EIS QSOB 77	004951.67	-29 14 27.4	20.57	0.05	> 1.85	0.22	3.07	0.23
EIS QSOB 78	004952.98	-29 53 06.2	20.66	0.08	> 2.85	0.25	2.49	0.26
EIS QSOB 79	004958.62	-29 14 03.7	20.99	0.07	> 1.85	0.20	2.51	0.21
EIS QSOB 80	004958.73	-29 20 59.2	20.81	0.06	> 1.84	0.20	2.74	0.21
EIS QSOB 81	005000.00	-29 25 02.3	20.14	0.04	> 1.70	0.16	3.17	0.17
EIS QSOB 82	005000.68	-29 51 25.5	20.90	0.09	> 2.47	0.31	2.61	0.32
EIS QSOB 83	005003.37	-29 15 42.8	20.24	0.04	> 2.49	0.18	2.53	0.19
EIS QSOB 84	005007.37	-29 27 32.0	20.87	0.10	> 2.31	0.12	1.92	0.15
EIS QSOB 85	005021.47	-29 25 45.1	20.46	0.04	> 2.37	0.20	2.79	0.20
EIS QSOB 86	005021.86	-29 17 41.1	20.52	0.05	> 2.23	0.16	2.54	0.17
EIS QSOB 87	005022.85	-29 15 49.1	19.56	0.02	> 2.32	0.13	3.22	0.13
EIS QSOB 88	005031.00	-29 41 24.1	20.78	0.05	> 2.65	0.21	2.69	0.22
EIS QSOB 89	005033.26	-29 23 05.9	19.61	0.02	> 2.68	0.12	3.23	0.12
EIS QSOB 90	005033.58	-29 20 01.3	20.25	0.04	> 2.75	0.11	2.27	0.12
EIS QSOB 91	005035.16	-29 17 13.0	20.90	0.07	> 2.07	0.22	2.38	0.23
EIS QSOB 92	005037.43	-29 23 27.0	20.78	0.05	> 1.73	0.24	3.13	0.25
EIS QSOB 93	005038.60	-29 42 07.1	20.50	0.04	> 2.61	0.22	3.02	0.23
EIS QSOB 94	005038.82	-29 51 50.7	20.77	0.08	> 2.54	0.29	2.76	0.30
EIS QSOB 95	005041.39	-29 17 30.1	20.14	0.05	> 2.30	0.18	2.39	0.18
EIS QSOB 96	005044.83	-29 43 47.3	20.33	0.05	> 2.73	0.29	2.91	0.29
EIS QSOB 97	005045.46	-29 33 29.2	20.31	0.03	> 2.37	0.20	3.29	0.20
EIS QSOB 98	005046.94	-29 15 53.2	20.45	0.05	> 2.22	0.16	2.29	0.17
EIS QSOB 99	005049.20	-29 25 09.1	20.03	0.03	> 3.28	0.12	2.75	0.12
EIS QSOB 100	005050.95	-29 18 47.6	19.93	0.03	> 2.43	0.10	2.57	0.11
EIS QSOB 101	005052.21	-29 49 32.7	20.81	0.07	> 1.90	0.31	3.25	0.32
EIS QSOB 102	005052.22	-29 44 25.6	20.76	0.06	> 2.35	0.22	2.99	0.23
EIS QSOB 103	005053.49	-29 43 55.5	21.00	0.07	> 2.62	0.29	2.54	0.30
EIS QSOB 104	005054.29	-29 14 03.6	20.27	0.04	> 2.13	0.19	2.55	0.20
EIS QSOB 105	005057.65	-29 31 51.1	20.93	0.05	> 2.37	0.22	2.79	0.23
EIS QSOB 106	005108.70	-29 47 35.6	20.46	0.04	> 2.12	0.37	3.41	0.37
EIS QSOB 107	005111.28	-29 44 35.2	20.77	0.07	> 2.36	0.20	2.81	0.22
EIS QSOB 108	005117.08	-29 33 22.8	20.76	0.05	> 2.46	0.21	2.78	0.21
EIS QSOB 109	005123.83	-29 49 15.5	20.77	0.05	> 2.51	0.22	2.87	0.22
EIS QSOB 110	005131.02	-29 45 49.3	20.53	0.04	> 2.20	0.36	3.35	0.37
EIS QSOB 111	005140.96	-29 36 54.3	20.67	0.05	> 3.09	0.16	2.19	0.17
EIS QSOB 112	005152.19	-29 40 27.9	20.89	0.06	> 2.44	0.23	2.77	0.23
EIS QSOB 113	005208.34	-29 43 02.0	20.78	0.06	> 2.25	0.33	2.98	0.33
EIS QSOB 114	005215.47	-29 35 56.2	20.52	0.04	> 2.30	0.32	3.15	0.32

Table 7. Continued.

ID	α (J2000.0)	δ	I	ε_I	(B-V)	$\varepsilon_{(B-V)}$	(V-I)	$\varepsilon_{(V-I)}$
EIS QSOB 115	005226.34	-294232.6	20.50	0.04	> 2.30	0.37	3.35	0.37
EIS QSOB 116	005229.75	-294519.1	20.38	0.05	> 3.22	0.22	2.32	0.22
EIS QSOB 117	005232.78	-293453.2	20.39	0.04	> 2.20	0.24	3.39	0.25
EIS QSOB 118	005238.19	-293339.5	20.80	0.05	> 2.28	0.22	2.86	0.22
EIS QSOB 119	005240.58	-293526.8	20.66	0.05	> 2.90	0.24	2.41	0.25
EIS QSOB 120	005246.61	-294314.5	20.47	0.04	> 3.16	0.22	2.49	0.22
EIS QSOB 121	005247.74	-293453.8	20.59	0.05	> 2.34	0.19	2.95	0.20
EIS QSOB 122	005310.88	-295211.2	20.26	0.04	> 2.86	0.24	2.94	0.25
EIS QSOB 123	005326.89	-294829.2	20.12	0.04	> 2.85	0.20	3.02	0.20
EIS QSOB 124	005333.13	-293644.2	20.87	0.06	> 2.69	0.20	2.35	0.21
EIS QSOB 125	005333.35	-294308.5	20.76	0.06	> 2.53	0.21	2.83	0.22
EIS QSOB 126	005334.50	-293623.8	20.70	0.05	> 2.17	0.22	3.08	0.23

Table 8. Quasar Candidates (low redshift).

ID	α (J2000.0)	δ	I	ϵ_I	(B-V)	$\epsilon_{(B-V)}$	(V-I)	$\epsilon_{(V-I)}$	Notes
EIS QLZ 1	004525.31	-293607.1	19.58	0.02	0.12	0.03	0.87	0.03	
EIS QLZ 2	004525.32	-293419.2	20.70	0.07	-0.02	0.06	0.65	0.09	
EIS QLZ 3	004540.31	-294035.8	19.68	0.03	0.15	0.02	0.61	0.04	
EIS QLZ 4	004545.07	-295232.3	21.13	0.08	0.23	0.10	0.76	0.10	
EIS QLZ 5	004601.42	-293040.0	20.15	0.04	0.22	0.04	0.74	0.05	
EIS QLZ 6	004612.25	-293110.3	19.10	0.02	0.11	0.02	0.79	0.02	ICS96 004345.8-294733
EIS QLZ 7	004616.10	-295010.9	17.86	0.00	0.22	0.01	0.68	0.01	QSO 0043-3006, $z = 1.124$
EIS QLZ 8	004623.24	-292137.0	20.35	0.04	0.14	0.05	0.87	0.05	
EIS QLZ 9	004623.78	-294832.9	19.26	0.02	0.17	0.02	0.78	0.02	
EIS QLZ 10	004630.57	-293959.2	20.51	0.07	0.22	0.06	0.88	0.08	
EIS QLZ 11	004637.56	-295325.2	20.22	0.04	-0.05	0.05	0.92	0.06	
EIS QLZ 12	004651.71	-292452.5	19.43	0.02	0.15	0.02	0.68	0.02	
EIS QLZ 13	004653.48	-292126.4	21.64	0.10	0.06	0.17	0.56	0.12	
EIS QLZ 14	004717.09	-295315.4	20.03	0.03	0.09	0.04	0.76	0.04	
EIS QLZ 15	004720.09	-295150.2	22.54	0.19	0.11	0.28	0.64	0.26	
EIS QLZ 16	004728.91	-291834.7	19.21	0.03	0.12	0.02	0.57	0.04	
EIS QLZ 17	004730.71	-294630.2	17.42	0.00	0.16	0.00	0.67	0.01	[CT83] 92, $z = 2.021$
EIS QLZ 18	004745.30	-293936.2	19.43	0.02	0.19	0.02	0.57	0.02	
EIS QLZ 19	004751.33	-294118.2	19.77	0.02	0.23	0.03	0.76	0.03	
EIS QLZ 20	004751.55	-293603.5	18.53	0.01	0.19	0.01	0.66	0.01	
EIS QLZ 21	004751.92	-294258.8	21.00	0.07	0.12	0.07	0.73	0.09	
EIS QLZ 22	004752.14	-292805.3	20.50	0.05	0.24	0.06	0.63	0.05	
EIS QLZ 23	004806.89	-291403.2	21.61	0.11	0.20	0.21	1.00	0.15	
EIS QLZ 24	004816.66	-292412.0	20.96	0.07	0.09	0.11	0.95	0.08	
EIS QLZ 25	004822.62	-293630.8	19.12	0.01	0.06	0.02	0.77	0.02	
EIS QLZ 26	004825.51	-295337.7	19.37	0.02	0.04	0.03	0.76	0.03	
EIS QLZ 27	004825.67	-293758.5	21.28	0.08	-0.24	0.11	0.91	0.12	
EIS QLZ 28	004839.50	-293558.9	19.40	0.02	0.12	0.02	0.66	0.02	
EIS QLZ 29	004906.47	-294046.1	20.00	0.03	0.12	0.03	0.71	0.04	
EIS QLZ 30	004907.34	-291812.6	20.48	0.04	0.22	0.06	0.74	0.06	
EIS QLZ 31	004949.67	-291655.0	19.71	0.02	0.00	0.04	0.86	0.03	
EIS QLZ 32	004958.15	-293312.6	20.92	0.05	0.12	0.07	0.77	0.07	
EIS QLZ 33	005000.15	-291911.6	21.17	0.08	0.16	0.15	0.88	0.11	
EIS QLZ 34	005005.11	-292502.1	20.36	0.04	0.06	0.05	0.77	0.05	
EIS QLZ 35	005012.81	-294032.1	20.15	0.03	0.19	0.04	0.72	0.04	
EIS QLZ 36	005025.10	-295101.7	19.96	0.04	0.07	0.04	0.86	0.05	
EIS QLZ 37	005028.11	-293126.1	19.41	0.02	0.21	0.02	0.54	0.02	
EIS QLZ 38	005033.18	-293613.7	19.70	0.02	0.11	0.02	0.68	0.03	
EIS QLZ 39	005041.81	-293615.9	18.56	0.01	0.11	0.01	0.73	0.01	QSO 0048-298, $z = 2.028$
EIS QLZ 40	005047.73	-292046.6	20.44	0.07	0.11	0.10	0.69	0.08	
EIS QLZ 41	005101.05	-294907.2	19.91	0.07	0.17	0.04	0.62	0.07	
EIS QLZ 42	005111.99	-295247.5	19.52	0.02	0.07	0.03	0.88	0.03	
EIS QLZ 43	005140.09	-294445.7	20.10	0.03	0.20	0.04	0.94	0.05	
EIS QLZ 44	005214.74	-293949.7	20.85	0.06	0.18	0.06	0.52	0.08	
EIS QLZ 45	005253.76	-294442.2	19.02	0.01	0.06	0.02	0.76	0.02	QSO 0050-300, $z = 1.922$
EIS QLZ 46	005327.75	-294538.5	19.21	0.02	0.17	0.02	0.81	0.02	QSO 0051-300, $z = 2.25$
EIS QLZ 47	005333.69	-294910.5	20.67	0.05	0.08	0.06	0.79	0.07	
EIS QLZ 48	005340.66	-294301.3	19.55	0.02	-0.06	0.03	0.84	0.03	